

See discussions, stats, and author profiles for this publication at: <https://www.researchgate.net/publication/47555084>

# pH Dependence of the Conformation of Small Peptides Investigated with Two-Dimensional Vibrational Spectroscopy

ARTICLE in THE JOURNAL OF PHYSICAL CHEMISTRY B · OCTOBER 2010

Impact Factor: 3.3 · DOI: 10.1021/jp105133r · Source: PubMed

---

CITATIONS

20

READS

43

## 3 AUTHORS:



Adriana Huerta Viga  
University of Colorado Boulder

12 PUBLICATIONS 77 CITATIONS

[SEE PROFILE](#)



Daniel Shaw  
University of Strathclyde

13 PUBLICATIONS 124 CITATIONS

[SEE PROFILE](#)



Sander Woutersen  
University of Amsterdam

103 PUBLICATIONS 4,303 CITATIONS

[SEE PROFILE](#)

# pH Dependence of the Conformation of Small Peptides Investigated with Two-Dimensional Vibrational Spectroscopy

Adriana Huerta-Viga, Daniel J. Shaw, and Sander Woutersen\*

Van't Hoff Institute for Molecular Sciences (HIMS), University of Amsterdam, Science Park 904, 1098XH, Amsterdam, The Netherlands

Received: June 4, 2010; Revised Manuscript Received: August 16, 2010

We investigate how the conformation of small peptides is influenced by the presence or absence of charge on the C-terminus and on the side groups. To this purpose, the conformations of two tripeptides, with acidic and basic side groups, is determined at several pD values using two-dimensional infrared (2DIR) spectroscopy. The investigated pD values are chosen relative to the C-terminal and side-chain  $pK_a$  values in such a way that the C-terminus and side groups are in well-defined protonation states. The measurements are analyzed quantitatively using an excitonic model for the Amide I' mode. From the vibrational coupling and the angle between the Amide I' transition dipoles obtained in this way, the dihedral angles ( $\phi, \psi$ ) of the central  $C_\alpha$  atom are determined. Interestingly, our measurements show that the backbone structure of the peptides is remarkably stable against changing the charges of both the side groups and the C-terminal carboxylate groups. This is probably a consequence of effective screening of the Coulomb interactions between the charged groups by the water molecules between them. We also find that the ( $\phi, \psi$ ) confidence regions obtained from 2DIR measurements can have highly irregular shapes as a consequence of the nonlinear relation between the dihedral angles and the experimentally determined Amide I' coupling and transition-dipole angle.

## Introduction

For many years, it was a general belief that short peptides did not adopt well-defined secondary structures in aqueous solution.<sup>1</sup> However, it has recently become clear that many peptides, even as short as trimers, have only a limited number of conformations in aqueous solution.<sup>1–4</sup> Resolving the conformations of these simple peptides is relevant because a plausible initial step in protein folding is the formation of local secondary structure, which can act as a nucleation site of the folding of an entire protein.<sup>1</sup> A systematic investigation of the preferred conformations of short amino-acid sequences and their dependence on environmental factors (e.g., pH, temperature, presence of denaturants) would make it possible to predict the location of such nucleation sites within a protein.

With commonly used experimental methods like nuclear magnetic resonance or circular dichroism, it is difficult to determine the conformation of small peptides unambiguously. In contrast, vibrational spectroscopy of the Amide I' mode (where the prime denotes N-deuteration of the peptide group) has proven to be well-suited for this task because its intrinsic time scale ( $\sim 1$  ps) is fast enough to separate coexisting conformers. In particular, 2DIR spectroscopy has emerged as a powerful method to determine peptide conformation in solution.<sup>5–14</sup> With this method, the conformation of a peptide is probed by measuring the coupling between the backbone Amide I' modes and the angles between Amide I' transition-dipole moments.

Here we apply this method to investigate the pH dependence of the conformation of two short peptides with acidic and basic side groups. The pH dependence of peptide conformations is of particular interest because the formation of amyloid peptide structures is known to depend on pH.<sup>15–17</sup> Recently, a combination of vibrational circular dichroism, Fourier transform infrared,

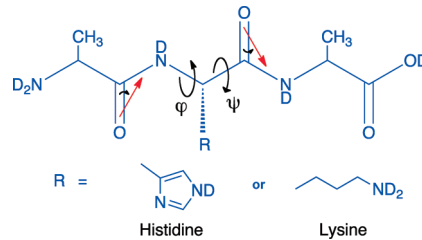


**Figure 1.** Molecular structure of the investigated tripeptides. The dihedral angles  $\varphi$  and  $\psi$  are shown as well as the transition dipole moment vectors (in red). The histidine and lysine side-chain groups (R) are depicted below the main structure of the tripeptide.

and Raman techniques has been used successfully to determine the secondary structure of small peptides.<sup>3,4,18–21</sup> On the basis of the reported changes of tripeptide conformations at different pH values reported in ref 3, our work focuses on the use of 2DIR spectroscopy to investigate the pH dependence in two alanine-based tripeptides, with basic (lysine) and acidic (histidine) side groups on the central  $C_\alpha$  atom. The molecular structure of these tripeptides is shown in Figure 1. In the Figure, the red arrows on the  $C=O$  bonds represent the transition dipole moments, which are at an angle of  $20^\circ$  with respect to these bonds due to the participation of the ND bend in the transition.<sup>22</sup> Also shown in the Figure are the dihedral angles  $\varphi$  and  $\psi$ , which are the source of essentially all of the interesting variability in protein conformation<sup>23</sup> and whose determination will be the central feature of this Article.

## Experimental Section

**Setup.** Pulses with a duration of 40 fs, centered at 800 nm, are generated using a commercially available mode-locked Ti:sapphire oscillator system whose output is amplified using a Ti:sapphire regenerative amplifier to obtain 800 nm pulses with

\* To whom correspondence should be addressed. E-mail: S.Woutersen@uva.nl.

a full width at half-maximum (fwhm) of 35 fs and an energy of 3.5 mJ at a 1 kHz repetition rate. These pulses are used to pump an optical parametric amplifier with two-stage parametric amplification in  $\beta\text{-BaB}_2\text{O}_4$  of a white light continuum and subsequent frequency difference generation in  $\text{AgGaS}_2$ . A nearly Gaussian spectrum is obtained in this manner, with a central wavelength that can be tuned from 2.5 to 12  $\mu\text{m}$ . For the measurements presented in this Article, only the 6  $\mu\text{m}$  region is used. At  $1640 \text{ cm}^{-1}$ , the energy, duration, and fwhm of the pulses are  $16 \mu\text{J}$ ,  $\leq 40$  fs, and  $315 \text{ cm}^{-1}$ , respectively.

To perform the measurements, we use a one-color pump–probe setup in which the beam is split into pump, probe, and reference pulses by means of a wedged  $\text{BaF}_2$  window. The majority of the power remains in the pump arm of the setup, which is passed through a FPI (Fabry–Perot interferometer) consisting of two partial-reflector mirrors, whose separation is adjusted with a feedback-controlled piezoelectric mount. The pulse energy and fwhm after the FPI are  $3 \mu\text{J}$  and  $10 \text{ cm}^{-1}$ , respectively. The polarization of the pump pulse is adjusted to be either parallel or perpendicular with respect to the probe by means of a zero-order  $\lambda/2$  plate. Using an off-axis parabolic mirror (10 cm focal length), all three beams are focused in the sample ( $\sim 200 \mu\text{m}$  focal diameter), and the pump and probe pulses are spatially overlapped. To determine the zero delay, a cross-correlation between the pump and probe beams is measured by means of two-photon absorption in InAs. The estimated temperature increase in the focal volume due to dissipation of the absorbed pump energy is  $\sim 0.5 \text{ K}$ .

The detection of the IR pulses is carried out with a  $\text{HgCdTe}$  detector-array onto which probe, pump, and reference beams are directed in a frequency-dispersed manner, resulting in a  $4 \text{ cm}^{-1}$  spectral resolution. This is also the resolution with which the central frequency of the narrow-band pump pulse can be adjusted. By comparing the transmitted probe spectrum in the presence and absence of the pump pulse, the pump-induced transient absorption change is measured. By scanning the pump frequency along a selected range with the FPI and measuring transient absorption spectra for each pump frequency, 2D vibrational spectra are constructed.

**Materials.** Two alanine-based tripeptides were investigated, L-alanyl-L-lysyl-L-alanine (AKA) and L-alanyl-L-histidyl-L-alanine (AHA). AKA was custom-synthesized by GL Biochem (>95% purity). TFA (trifluoroacetic acid) is commonly used as a solvent during synthesis and purification of peptides. Because it has a sharp and prominent absorption peak at  $1690 \text{ cm}^{-1}$ , it needs to be removed. To eliminate TFA, the peptide was repeatedly freeze-dried from a 0.1 M solution of DCI in  $\text{D}_2\text{O}$ , allowing simultaneous hydrogen–deuterium exchange of the NH groups. AHA was purchased from Bachem Bioscience (>98% purity) and was used without further purification. Hydrogen–deuterium exchange is achieved in a similar manner by repeatedly freeze-drying from a small volume of  $\text{D}_2\text{O}$ .

Both peptides were dissolved in  $\text{D}_2\text{O}$  to obtain a 300 mM concentration. Aggregation was not observed in the IR spectra, in agreement with previous studies of similar peptides at comparable concentrations.<sup>24</sup> The pD was determined using a pH meter together with a Micro pH electrode. To obtain the pD value, 0.4 was added to the direct reading of the meter according to a pH–pD calibration previously reported.<sup>25</sup> To change the pD of the samples, aliquots of NaOD or DCI were added until the desired pD value was reached. When measuring, droplets of the samples were placed between 2 mm thick  $\text{CaF}_2$  windows, separated by a 25  $\mu\text{m}$  Teflon spacer (except for the

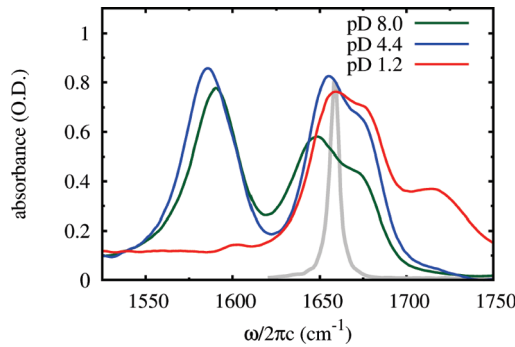


**Figure 2.** Solvent-subtracted linear absorption spectra of AHA at three different pD values below and above the  $pK_a$  values of the histidine side chain ( $pK_a = 6.04$ ) and the C-terminal carboxylate ( $pK_a = 2.35$ ). The gray line is a representative pump–pulse spectrum (scaled).

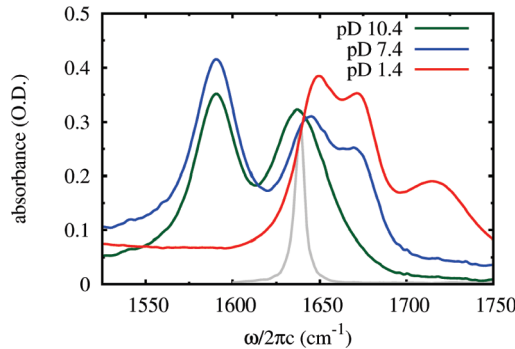


**Figure 3.** Solvent-subtracted linear absorption spectra of AKA at three different pD values below and above the  $pK_a$  values of the lysine side chain ( $pK_a = 9.18$ ) and the C-terminal carboxylate ( $pK_a = 2.35$ ). The gray line is a representative pump–pulse spectrum (scaled).

linear absorption spectrum of AHA at pD 4.4 in Figure 2, which was measured with a 50  $\mu\text{m}$  spacer).

## Results

**Linear Absorption Spectra.** As can be seen in Figures 2 and 3, the Amide I' linear spectrum of both peptides in the  $1620\text{--}1700 \text{ cm}^{-1}$  region consists of two peaks, each corresponding to a peptide bond. The high and low frequency Amide I' bands correspond to the peptide groups closer to the N- and C-terminus, respectively.<sup>26</sup> The histidine side chain has a  $pK_a$  of 6.04,<sup>27</sup> and alanine has a carboxylic acid  $pK_a$  of 2.35.<sup>27</sup> pD values below and above these thresholds were chosen to observe the change in conformation upon protonation of the side-chain and the C-terminus. At pD 1.2, when both the side chain and the C-terminus are protonated, there is a weak band at  $1600 \text{ cm}^{-1}$ , which arises from the histidine imidazole side-chain stretch.<sup>28</sup> The Amide I' modes are centered at  $1658$  and  $1675 \text{ cm}^{-1}$ , and the carboxylic acid band is at  $1710 \text{ cm}^{-1}$ . When the pD is increased to 4.4, the C-terminus is deprotonated. As a consequence, the C=O stretch band of the carboxylate appears at  $1585 \text{ cm}^{-1}$ , and the  $1710 \text{ cm}^{-1}$  carboxylic acid band disappears. The  $1600 \text{ cm}^{-1}$  band remains in the same position and can be seen as a shoulder on the carboxylate band. The  $1675 \text{ cm}^{-1}$  band remains at the same position, and the  $1658 \text{ cm}^{-1}$  apparently shifts to a lower frequency, but this is due to the carboxylate band appearance that raises the band. At pD 8.0, the histidine side-chain is deprotonated, and as a result, the  $1600 \text{ cm}^{-1}$  band shifts to  $1570 \text{ cm}^{-1}$ .<sup>28</sup> However, the absorption cross section of the shifted band is so much smaller that it is not visible in the Figure. The Amide I' bands remain at the same frequency.

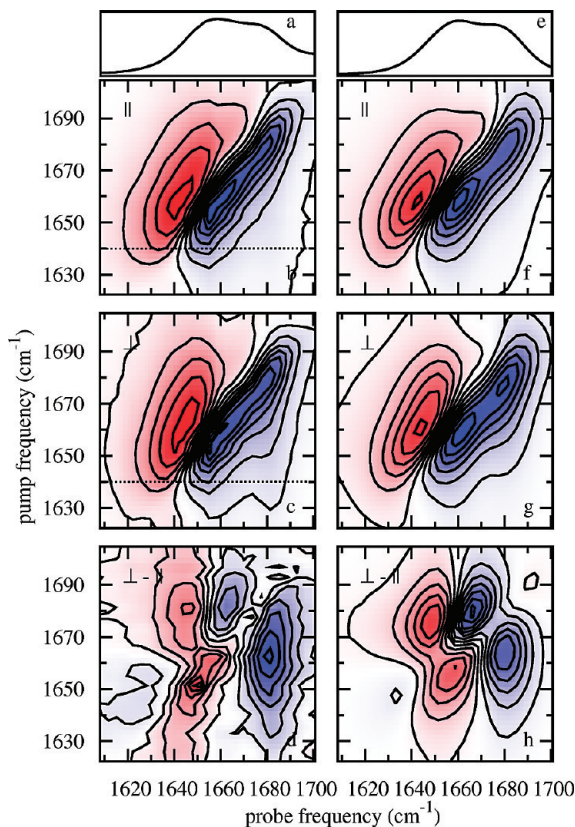


**Figure 4.** Left column: experimental 2DIR spectra of AHA at pD 1.2 at a pump–probe delay of 0.9 ps. Right column: global least-squares fit to the data. Blue and red colors indicate negative and positive absorption changes, respectively. (a,e) Linear spectra. (b,f) Absorption change versus pump and probe frequencies for parallel polarizations of the pump and probe pulses; contour intervals are 0.35 mOD. (c,g) Same for perpendicular polarizations of the pump and probe pulses; contour intervals are 0.12 mOD. (d,h) Weighted difference  $2.70\Delta\alpha_{\perp} - \Delta\alpha_{\parallel}$  between perpendicular and parallel measurements; contour intervals are 0.06 mOD.

The lysine side-chain  $pK_a$  has a value of 9.18.<sup>27</sup> This value and the alanine carboxylic acid  $pK_a$  (2.35) were used as thresholds for varying the pD of the trimer. At pD 1.2, the lysine side chain and the C-terminus are both protonated, and as a consequence, the carboxylic acid band can be seen at  $1710\text{ cm}^{-1}$ . The Amide I' modes are located at  $1648$  and  $1671\text{ cm}^{-1}$ . At pD 7.4, the C-terminus is protonated and the carboxylate band appears at  $1590\text{ cm}^{-1}$ , whereas the carboxylic acid disappears. The Amide I' bands remain at the same frequency. At pD 10.4, the lysine side chain is deprotonated, and as a result, the two Amide I' bands merge into a single one, possibly because of hydrogen bonding with the N-terminus. The fact that both bands are on top of each other makes the analysis of the 2D data impossible and therefore this pD value was no longer considered.

**2D Pump–Probe Spectra.** To determine how the conformation changes when the side group and C-terminus are protonated, 2DIR measurements were performed on both trimers for each of the relevant pD values described in the previous section. Figure 4b,c shows the results for AHA at pD 1.2 for parallel and perpendicular polarizations of the pump and probe pulses. At this pD, both the histidine side group and the C-terminus are protonated. Along the diagonal, the negative (blue) signal corresponds to the ground-state bleaching and  $\nu = 1 \rightarrow 0$  stimulated emission of each of the two Amide I' modes, and the positive (red) signal is the corresponding  $\nu = 1 \rightarrow 2$  induced absorption. The perpendicular measurement shows more inten-

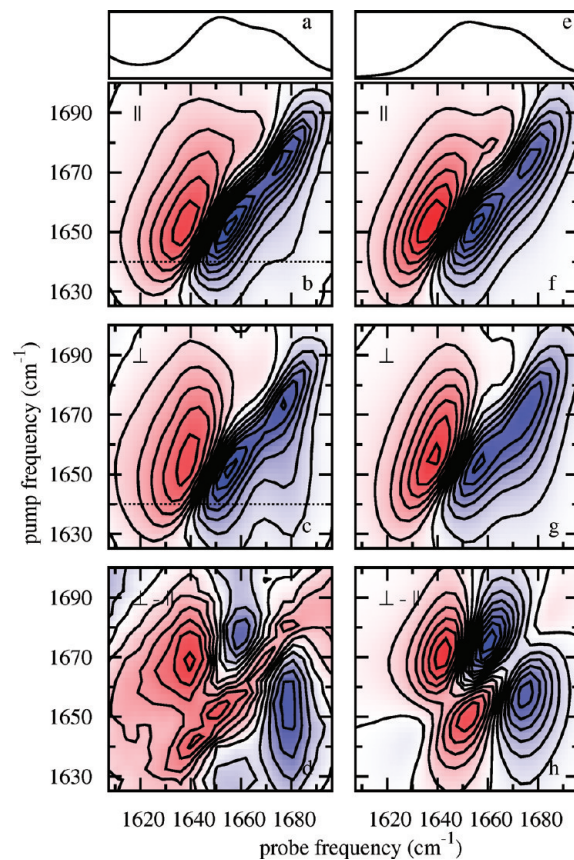


**Figure 5.** Left column: experimental 2DIR spectra of AHA at pD 4.4 at a pump–probe delay of 1.2 ps. Right column: global least-squares fit to the data. Blue and red colors indicate negative and positive absorption changes, respectively. (a,e) Linear spectra. (b,f) Absorption change versus pump and probe frequencies for parallel polarizations of the pump and probe pulses; contour intervals are 0.4 mOD. (c,g) Same for perpendicular polarizations of the pump and probe pulses; contour intervals are 0.19 mOD. (d,h) Weighted difference  $2.45\Delta\alpha_{\perp} - \Delta\alpha_{\parallel}$  between perpendicular and parallel measurements; contour intervals are 0.1 mOD.

sity in the off-diagonal region, which indicates that the modes are coupled and that the angle between the coupled transition dipole moments is nonzero.<sup>6</sup> The cross-peaks are more prominent in the perpendicular measurement because they have a different anisotropy compared with the diagonal peaks, provided that the angle between the coupled transition dipole moments is nonzero.<sup>26</sup> To observe the cross peaks more clearly, a subtraction of perpendicular and parallel signals is performed. [In theory, this difference spectrum should be constructed by subtracting the parallel measurement from three times the perpendicular one due to anisotropy considerations.<sup>8</sup> In the peptides that we investigated, the overlap between cross- and diagonal peaks is such that this ratio is different from three. In addition, small parallel displacements of the pump beam upon changing the polarization that lead to an overall reduction of the signal intensity may also affect this ratio. For this reason, the ratio is determined from the maxima of both measurements.] The result is seen in Figure 4d, in which we can see that each cross peak is composed of a positive and negative component. The cross-peaks arise from the coupling between the Amide I' modes and can be explained as follows. In first-order approximation, the coupling between the modes causes an anharmonic frequency shift of one of the modes when the other is excited to the  $\nu = 1$  state.<sup>6</sup> Because this shift is generally smaller than the line width of the probed

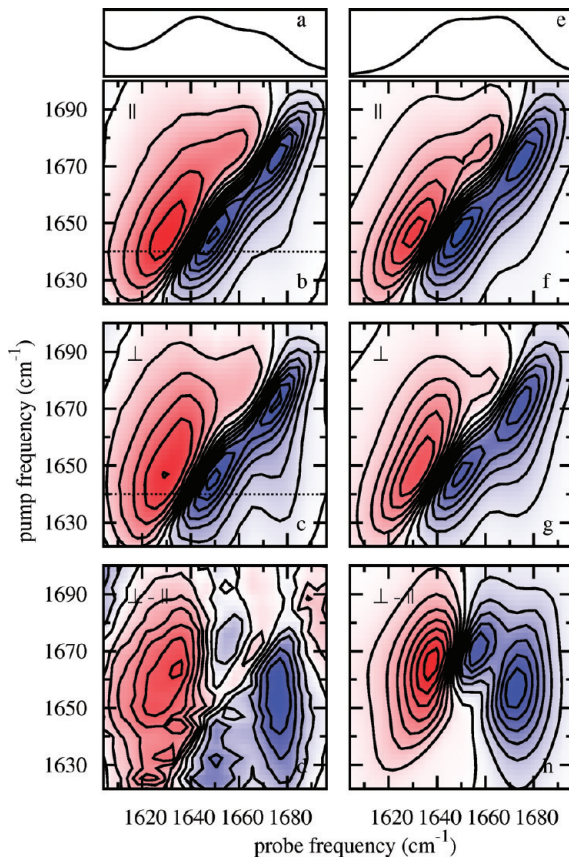


**Figure 6.** Left column: experimental 2DIR spectra of AHA at pD 8.0 at a pump–probe delay of 1.2 ps. Right column: global least-squares fit to the data. Blue and red colors indicate negative and positive absorption changes, respectively. (a,e) Linear spectra. (b,f) Absorption change versus pump and probe frequencies for parallel polarizations of the pump and probe pulses; contour intervals are 0.4 mOD. (c,g) Same for perpendicular polarizations of the pump and probe pulses; contour intervals are 0.17 mOD. (d,h) Weighted difference  $2.70\Delta\alpha_{\perp} - \Delta\alpha_{\parallel}$  between perpendicular and parallel measurements; contour intervals are 0.1 mOD.

transition, the line shape of the cross peaks along the probe axis is approximately given by the derivative of the absorption band and thus exhibits a negative (bleach) and a positive (excited-state absorption) part on the high- and low-frequency sides, respectively.

The corresponding plots for AHA at pD 4.4 are shown in Figure 5a–d. At this pD, the histidine side chain is still protonated, but the C terminus is deprotonated. It can be seen from Figure 5d that the cross-peaks are more visible because the separation between the Amide I' bands is larger than that at pD 1.2. When the pD is further increased to 8.0 so that both the histidine side chain and the C-terminus are deprotonated, the cross-peaks retain the same magnitude but change shape, as can be seen in Figure 6.

A comparison of the relative magnitude of the cross-peaks at different pD values can be seen in Figure 7, where a cross-section of the 2D plot is shown for both parallel and perpendicular polarizations. (The scaling factor between them is indicated in the captions of Figures 4–6.)

Compared with AHA, AKA shows a different pD dependence. When deprotonating the C-terminal carboxylate by increasing the pD from 1.4 to 7.4, a smaller change is observed between the corresponding parallel and perpendicular measurements, as compared with AHA, shown in Figures 8b,c and 9b,c.

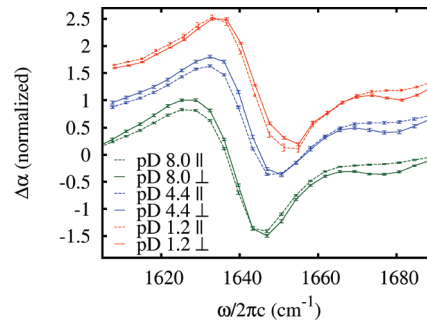


**Figure 7.** Cross section through the perpendicular 2D-IR spectra of AHA at pD values of 8.0, 4.4, and 1.2 at a pump frequency of 1640 cm⁻¹, indicated by the dotted line in Figures 4–6. The data points have been normalized and displaced.

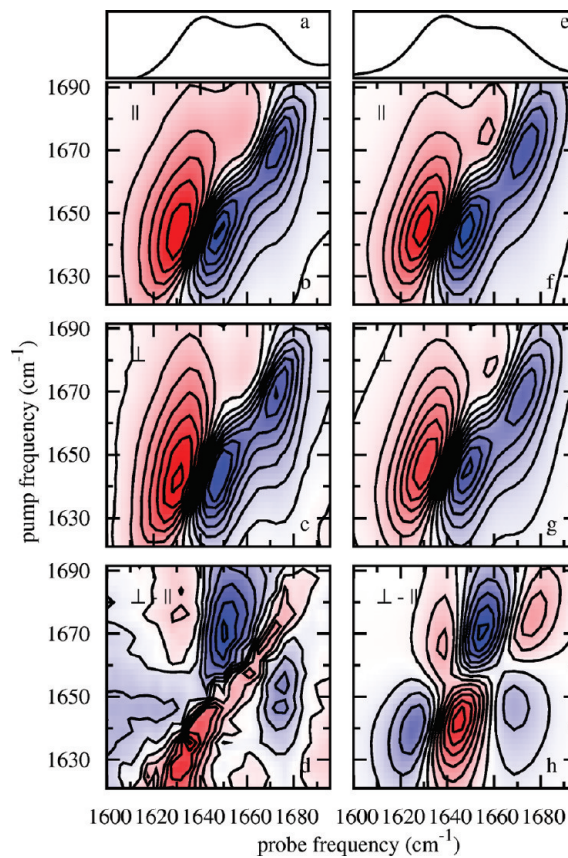


**Figure 8.** Left column: experimental 2DIR spectra of AKA at pD 1.4 at a pump–probe delay of 1 ps. Right column: global least-squares fit to the data. Blue and red colors indicate negative and positive absorption changes, respectively. (a,e) Linear spectra. (b,f) Absorption change versus pump and probe frequencies for parallel polarizations of the pump and probe pulses; contour intervals are 0.35 mOD. (c,g) Same for perpendicular polarizations of the pump and probe pulses; contour intervals are 0.15 mOD. (d,h) Weighted difference  $1.93\Delta\alpha_{\perp} - \Delta\alpha_{\parallel}$  between perpendicular and parallel measurements; contour intervals are 0.06 mOD.

The magnitude and shape of the cross-peaks also remain almost unchanged. (See Figures 8d and 9d.)

### Quantitative Analysis

**Model.** In the theoretical treatment, we assume the existence of a single dominant ( $\varphi, \psi$ ) conformation of the peptides in solution. This assumption is supported by experimental and

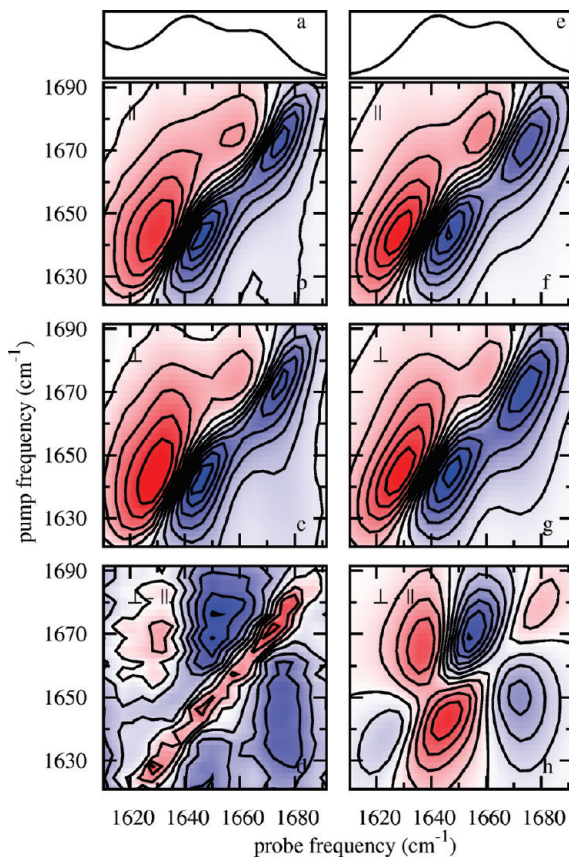


**Figure 9.** Left column: experimental 2DIR spectra of AKA at pH 7.4 at a pump–probe delay of 1 ps. Right column: global least-squares fit to the data. Blue and red colors indicate negative and positive absorption changes, respectively. (a,e) Linear spectra. (b,f) Absorption change versus pump and probe frequencies for parallel polarizations of the pump and probe pulses; contour intervals are 0.3 mOD. (c,g) Same for perpendicular polarizations of the pump and probe pulses; contour intervals are 0.15 mOD. (d,h) Weighted difference  $1.93\Delta\alpha_{\perp} - \Delta\alpha_{\parallel}$  between perpendicular and parallel measurements; contour intervals are 0.05 mOD.

molecular dynamics studies on other short peptides,<sup>29–31</sup> where single dominant conformations were also found. The good agreement between the experimental and calculated 2D-IR spectra (Figures 4–9) suggests that this assumption is valid. We do take into account the fact that each molecule is in a different solvent environment (inhomogeneous broadening, see eqs 7 and 8).

We analyze the data using an excitonic model for the Amide I' band, which assumes the Amide I' modes of the peptide to be coupled anharmonic oscillators. This model has been proven to describe accurately both the linear<sup>21,32–34</sup> and third-order nonlinear<sup>5</sup> response of coupled Amide I' vibrations in peptides and proteins. For resonant pump–probe experiments, it is sufficient to consider only one- and two-exciton states.<sup>35</sup> Three-exciton states are not observed because the pump intensity is not sufficient to populate the second excited state. (With our pump intensity, the  $\nu = 2$  population is <1% of the  $\nu = 1$  population.) The linear response is related to the first-order polarization, and the nonlinear pump–probe signal is related to the third-order polarization by<sup>35</sup>

$$\Delta\alpha^{2D} = \text{Im}[E_2^*(\omega) \cdot \mathbf{P}^{(3)}(\omega)] \quad (1)$$

where  $E_2(\omega)$  is the probe field (modeled with a Dirac delta function in time) and  $\mathbf{P}^{(3)}(\omega)$  is the third-order induced polarization. The pump pulse is modeled as a single-sided exponential. The induced polarization  $\mathbf{P}(t)$ , which is a bulk property, is calculated from the ensemble average of its corresponding molecular property, the transition dipole moment  $\hat{\mu}(t)$ . The eigenstates of a noninteracting system of two harmonic oscillators are used as a basis set, which is ordered as follows

$$\{|0,0\rangle, |1,0\rangle, |0,1\rangle, |2,0\rangle, |0,2\rangle, |1,1\rangle\} \quad (2)$$

Assuming that the coupling  $\beta$  between the Amide I' modes is bilinear in the displacements,<sup>5</sup> and introducing the anharmonicity of the Amide I' potential in a phenomenological way, one obtains a Hamiltonian given by

$$H = \begin{pmatrix} 0 & & & \\ \hline & \epsilon_1 & \beta & \\ & \beta & \epsilon_2 & \\ \hline & 2\epsilon_1 - \Delta & 0 & \sqrt{2}\beta \\ & 0 & 2\epsilon_2 - \Delta & \sqrt{2}\beta \\ & \sqrt{2}\beta & \sqrt{2}\beta & \epsilon_1 + \epsilon_2 \end{pmatrix}, \quad (3)$$

where the zero-, one-, and two-exciton manifolds are separated by lines. The coupling  $\beta$  appears only in off-diagonal terms. In this Hamiltonian, the diagonal elements correspond to the eigenvalues of the uncoupled system, except for the shift  $\Delta$  in the two-exciton energy for a single-oscillator state. A harmonic approximation has been taken for the amplitudes of the  $\nu = 0 \rightarrow 1$  and  $1 \rightarrow 2$  transitions, that is,  $\langle 2,0|H|1,1\rangle = \sqrt{2}\langle 1,0|H|0,1\rangle$ , etc. When diagonalizing the Hamiltonian in eq 3, the zero-, one- and two-exciton manifolds do not mix, so that the new  $n$ -exciton states (which form a new basis, constructed from the basis of eq 2 by a unitary transformation) are linear combinations of the uncoupled  $n$ -exciton states. When the coupling is small compared with the frequency splitting ( $|\beta| \ll |\epsilon_1 - \epsilon_2|$ ), the exciton states are localized mainly on single Amide I' oscillators. In the opposite case, they are delocalized over both oscillators. Correspondingly, the eigenenergies,  $\Omega_i$ , will be similar to, or different from the uncoupled energies depending on the strength of the coupling.

The transition-dipole vectors of the uncoupled states are  $\boldsymbol{\mu}_1$  and  $\boldsymbol{\mu}_2$ , and they are at an angle  $\theta$ . Using these vectors, the transition-dipole moment matrix, written on the basis of eq 2, and in the harmonic approximation is given by

$$\hat{\mu} = \begin{pmatrix} & \boldsymbol{\mu}_1 & \boldsymbol{\mu}_2 & & \\ \hline \boldsymbol{\mu}_1 & & & \sqrt{2}\boldsymbol{\mu}_1 & 0 & \boldsymbol{\mu}_2 \\ \boldsymbol{\mu}_2 & & & 0 & \sqrt{2}\boldsymbol{\mu}_2 & \boldsymbol{\mu}_1 \\ \hline & \sqrt{2}\boldsymbol{\mu}_1 & 0 & & & \\ & 0 & \sqrt{2}\boldsymbol{\mu}_2 & & & \\ & \boldsymbol{\mu}_2 & \boldsymbol{\mu}_1 & & & \end{pmatrix}. \quad (4)$$

This matrix needs to be written in the basis of the coupled system using a similarity transformation to get  $\hat{\mu}_{\text{exc}}$ . The elements  $\boldsymbol{\mu}_{0i}$  of  $\hat{\mu}_{\text{exc}}$  are the  $\nu = 0 \rightarrow 1$  transition dipoles of the transitions from the ground state to the  $|li\rangle$  ( $i \in \{2,3\}$ ) one-exciton

**TABLE 1: Fit Parameters of the 2D Measurements<sup>a</sup>**

| parameter                                 | AHA <sup>pD1</sup> | AHA <sup>pD4</sup> | AHA <sup>pD8</sup> | AKA <sup>pD1</sup> | AKA <sup>pD7</sup> |
|---|--------------------|--------------------|--------------------|--------------------|--------------------|
| $\chi_r^2$                                | 42                 | 20                 | 27                 | 33                 | 55                 |
| $\bar{\varepsilon}_1$ (cm <sup>-1</sup> ) | 1658 ± 3           | 1654               | 1647               | 1645               | 1644               |
| $\bar{\varepsilon}_2$ (cm <sup>-1</sup> ) | 1678 ± 4           | 1673               | 1671               | 1669               | 1670               |
| $\beta$ (cm <sup>-1</sup> )               | 4.0 + 1.6/-1.9     | 4.9 + 1.7/-2.0     | 4.9 + 2.0/-2.4     | 3.5 + 1.8/-2.1     | 4.1 + 2.2/-2.6     |
| $\theta$                                  | 112 + 15/-17       | 103 ± 11           | 104 + 12/-13       | 106 + 16/-14       | 106 + 17/-15       |
| $\gamma_{10}$ (cm <sup>-1</sup> )         | 5.1 + 1.5/-1.3     | 4.5                | 4.6                | 5.2                | 5.0                |
| $\gamma_{12}$ (cm <sup>-1</sup> )         | 8.2 + 2.8/-2.2     | 7.2+               | 7.0                | 6.8                | 6.7                |
| $\delta_1$ (cm <sup>-1</sup> )            | 22 + 7/-5          | 23                 | 26                 | 20                 | 22                 |
| $\delta_2$ (cm <sup>-1</sup> )            | 17 + 10/-7         | 22                 | 22                 | 22                 | 21                 |
| $\Gamma$ (cm <sup>-1</sup> )              | 3.5 <sub>f</sub>   | 5.3 <sub>f</sub>   | 5.0 <sub>f</sub>   | 7.3 <sub>f</sub>   | 5.0 <sub>f</sub>   |

<sup>a</sup> Subindex *f* labels parameters kept fixed during the fit.

states. The elements  $\mu_{ik}$  are the transition-dipole of the  $\nu = 1 \rightarrow 2$  transitions from the one-exciton state  $|i\rangle$  to the two-exciton state  $|k\rangle$  ( $i \in \{2,3\}$  and  $k \in \{4,5,6\}$ ). The elements  $\mu_{mn}$  of this matrix and the eigenenergies  $\Omega_m$  of the coupled states are all that is needed to calculate the infrared spectrum and the third-order response of the system. For the linear spectra, only the  $\nu = 0 \rightarrow 1$  transitions have to be taken into account. The linear absorption of a particular molecule with localized frequencies  $\varepsilon_1$  and  $\varepsilon_2$  is given by

$$\alpha_{\varepsilon_1, \varepsilon_2}(\omega) = \sum_i \frac{|\mu_{0i}|^2 \gamma_{01}}{(\omega - \Omega_i)^2 + \gamma_{01}^2} \quad (5)$$

where the  $\Omega_i$  depend parametrically on  $\varepsilon_1$  and  $\varepsilon_2$  and where  $\gamma_{01}$  is the homogeneous dephasing rate assumed to be the same for both oscillators.

For the nonlinear pump–probe response, the  $\nu = 1 \rightarrow 2$  transitions also play a role. Using a perturbative approach,<sup>5,8,35</sup> the pump–probe signal is given by

$$\Delta\alpha_{\varepsilon_1, \varepsilon_2}^{2D}(\omega_{\text{pump}}, \omega_{\text{probe}}) = -\frac{\gamma_{01}(1 + \gamma_{01}/\Gamma)}{15\hbar^3} \times \\ \left\{ \sum_i \frac{p_2 |\mu_{0i}|^2 |\mu_{0i}|^2 + p_1 |\mu_{0i}|^2 |\mu_{0i}|^2}{[(\omega_{\text{pump}} - \Omega_i)^2 + (\gamma_{01} + \Gamma)^2][(\omega_{\text{probe}} - \Omega_i)^2 + \gamma_{01}^2]} \right. \\ + \sum_{ij} \frac{p_2 |\mu_{0i}|^2 |\mu_{0j}|^2 + p_1 (\mu_{0i} \cdot \mu_{0j})^2}{[(\omega_{\text{pump}} - \Omega_i)^2 + (\gamma_{01} + \Gamma)^2][(\omega_{\text{probe}} - \Omega_j)^2 + \gamma_{01}^2]} \\ \left. - \sum_{i,k} \frac{p_2 |\mu_{ik}|^2 |\mu_{0i}|^2 + p_1 (\mu_{ik} \cdot \mu_{0i})^2}{[(\omega_{\text{pump}} - \Omega_i)^2 + (\gamma_{12} + \Gamma)^2][(\omega_{\text{probe}} - (\Omega_k - \Omega_i))^2 + \gamma_{12}^2]} \right\} \quad (6)$$

where  $i, j \in \{2,3\}$  and  $k \in \{4,5,6\}$ . The first term in this equation represents the contribution to the pump–probe signal due to ground-state bleaching, the second stimulated emission, and the third excited-state absorption.  $\gamma_{12}$  is the homogeneous dephasing rate of the  $\nu = 1 \rightarrow 2$  transitions.  $\Gamma$  is the half width at half-maximum of the pump spectrum, which is inversely proportional to its duration. The factors  $p_1 = 2, 1$  and  $p_2 = -1, 2$  are used for parallel and perpendicular angles between pump and probe polarizations, respectively.

The fact that we measure on an ensemble of molecules in different solvent surroundings is taken into account in both the linear and nonlinear responses. Following the central limit theorem,<sup>36</sup> the localized Amide I' frequencies  $\varepsilon_1$  and  $\varepsilon_2$  of this ensemble are considered to have Gaussian probability distributions around central values  $\bar{\varepsilon}_1$  and  $\bar{\varepsilon}_2$ , such that the linear and nonlinear absorption become

$$\alpha_{\bar{\varepsilon}_1, \bar{\varepsilon}_2}(\omega) = \iint d\varepsilon_1 d\varepsilon_2 e^{(\varepsilon_1 - \bar{\varepsilon}_1)^2/\delta_1^2} e^{(\varepsilon_2 - \bar{\varepsilon}_2)^2/\delta_2^2} \alpha_{\varepsilon_1, \varepsilon_2}(\omega) \quad (7)$$

and

$$\Delta\alpha_{\bar{\varepsilon}_1, \bar{\varepsilon}_2}^{2D}(\omega_{\text{pump}}, \omega_{\text{probe}}) = \iint d\varepsilon_1 d\varepsilon_2 e^{(\varepsilon_1 - \bar{\varepsilon}_1)^2/\delta_1^2} e^{(\varepsilon_2 - \bar{\varepsilon}_2)^2/\delta_2^2} \Delta\alpha_{\varepsilon_1, \varepsilon_2}^{2D}(\omega_{\text{pump}}, \omega_{\text{probe}}) \quad (8)$$

where  $\delta_1$  and  $\delta_2$  are the inhomogeneous widths.

**Least-Squares Fit.** The fitting routine uses the Levenberg–Marquardt method to minimize  $\chi^2 = \sum_{i=1}^N [(y_i^{\text{exptl}} - y_i^{\text{calcd}})/(\sigma_i)]^2$ , where the measured points are  $y_i^{\text{exptl}}$  (with corresponding standard deviations  $\sigma_i$ ), whereas  $y_i^{\text{calcd}}$  represents the calculated values (which depend on the fitting parameters). The fit was performed simultaneously on the parallel and perpendicular 2D-IR measurements, using an independent overall scaling factor for each. In this manner, the diagonal peaks calibrate the scaling factor, and it is possible to extract the cross-peak anisotropy-related information in an accurate manner. The outcome of the fits to the 2D measurements are presented in the right column of Figures 4–9. A rule of thumb for a good fit is when the reduced chi square  $\chi_r^2 = \chi^2/(N - M)$  has a value  $\sim 1$  ( $N$  being the number of data points and  $M$  being the number of parameters).<sup>37</sup> It has to be kept in mind that the model is not linear in the parameters and that several simplifications have been made. However, we find that the fits reproduce the relevant features of the measurements quite well, although the  $\chi_r^2$  is significantly larger than 1. The parameters obtained from the fit are shown in Table 1 as well as the corresponding  $\chi_r^2$ . The width of the pump spectrum  $\Gamma$  was determined experimentally and was treated as a fixed parameter in the fits. The magnitudes of the local transition-dipole moments ( $\mu_1$  and  $\mu_2$  in eq 4) of the uncoupled oscillators were assumed to be equal based on a DFT normal mode calculation, which we performed on a Gly–Gly–Gly neutral peptide with the B3LYP functional and the +G(d,p) basis set. From this calculation, we found the difference between the transition-dipole magnitudes to be <4%. Following literature reported values,<sup>38</sup> a value of 12 cm<sup>-1</sup> was used for the anharmonicity. In ref 5, a value of  $\Delta = 16$  cm<sup>-1</sup> was employed, but using this value resulted in significantly larger  $\chi_r^2$  values (50% larger than the ones reported here). This difference can be accounted for by the fact that in ref 5 DMSO (dimethylsulfoxide) was used as the solvent, whereas in ref 38, DMSO:D<sub>2</sub>O 1:1 mixture was employed. Hence, one would indeed expect an anharmonicity closer to 12 cm<sup>-1</sup> when working with pure D<sub>2</sub>O as a solvent. The values for the homogeneous widths  $\gamma_{01}$  and  $\gamma_{12}$  are in agreement with previous studies in Amide I' modes ( $\sim 6$  cm<sup>-1</sup>),<sup>39</sup> and the same holds for the

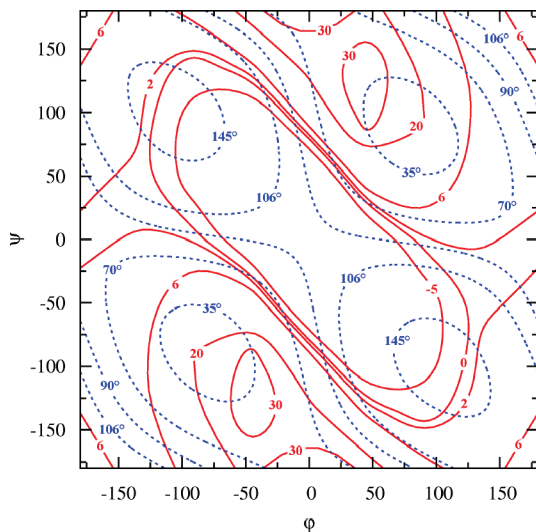


**Figure 10.** Ramachandran plot of the angle  $\theta$  (in degrees, blue contours) and the coupling  $\beta$  (in inverse centimeters, red contours, taken from ref 40) between transition dipole moments as function of the dihedral angles  $\phi$  and  $\psi$  defined in Figure 1.

inhomogeneous widths  $\delta_1$  and  $\delta_2$  ( $\sim 25 \text{ cm}^{-1}$ ).<sup>6</sup> To obtain an estimate for the uncertainties in the parameter values, we proceed as follows. The outcome of a  $\chi^2$  minimization routine is the covariance matrix, which is related to the confidence limits of the fitted parameters, but the values of  $\chi^2_r$  that we obtained are too large to follow this procedure. (The resulting uncertainties are unrealistically small.) An estimation of the confidence limits was therefore performed by increasing or decreasing the parameter until the  $\chi^2_r$  was doubled. These confidence limits of  $\beta$  and  $\theta$  were used to construct Figure 11, as will be explained in the next section.

**Peptide Conformations.** The conformation of a peptide is completely characterized by specifying three dihedral angles for each residue.<sup>41</sup> Two of them are  $\phi$  and  $\psi$ , illustrated in Figure 1, which describe rotations about the N–C<sub>α</sub> and C<sub>α</sub>–C' bonds, respectively. The third angle,  $\omega$ , describes a rotation about the C'–N peptide bond and is always close to 180° because of the partial double-bond character of this bond and sterical hindrance considerations.<sup>41</sup> We look at the central C<sub>α</sub> atom as its dihedral angles completely characterize the conformation of the trimer. It has been previously shown<sup>8,20</sup> that it is possible to determine ( $\phi, \psi$ ) from the experimentally observed ( $\beta, \theta$ ) (the coupling between the Amide I' transition dipole moments and the angle  $\beta$  between them) because there is a functional relation between these two pairs of parameters. A graphical representation of this functional relation is shown in Figure 10. The blue contours represent values for the angle  $\theta$  at all possible ( $\phi, \psi$ ) combinations. We obtained these values by assuming a 20° angle between the C=O axis and the transition dipole, as shown in Figure 1.<sup>22</sup> The red contours represent values for the coupling  $\beta$  at different ( $\phi, \psi$ ), which were obtained using an ab initio normal mode calculation at the B3LYP,6-31+G\* level on the glycine dipeptide (CH<sub>3</sub>–CONH–CH<sub>2</sub>–CONH–CH<sub>3</sub>), as reported in ref 40. Glycine is generally chosen for this type of calculation<sup>42–47</sup> because it is the only amino acid that has a sufficiently small side group for the complete ( $\phi, \psi$ ) conformational space to be explored. (All other residues are larger and consequently experience sterical hindrance in a large ( $\phi, \psi$ ) region.) Compared with diglycine, the two peptides investigated here are different: they have a slightly longer backbone and larger side groups, and they are charged. However, a systematic investigation using DFT calculations<sup>46</sup> on a series of tripeptides

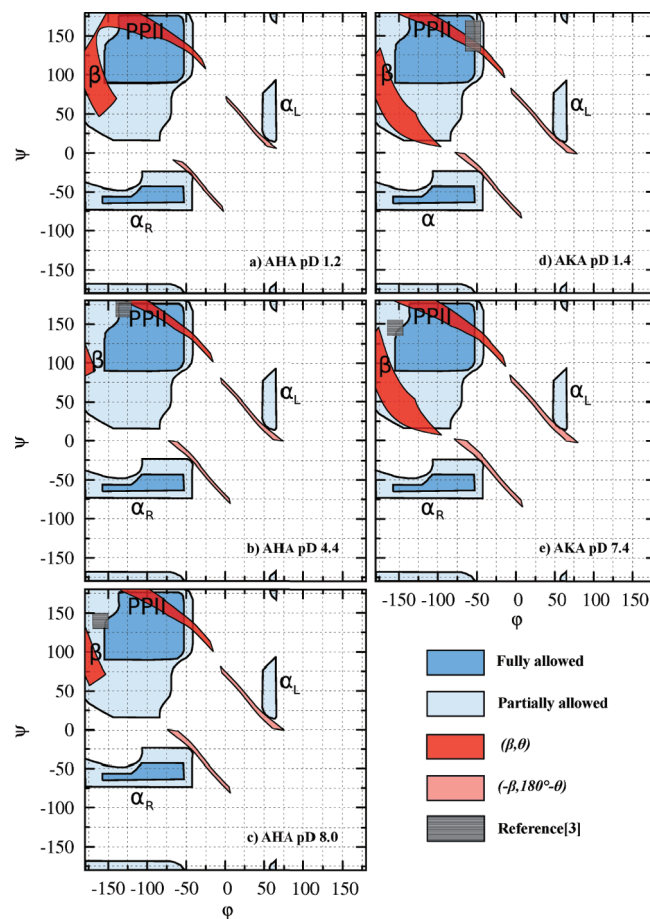


**Figure 11.** Map of the overlap between the allowed zoned by sterical hindrance (blue, taken from ref 41) and the confidence regions obtained from the fit (red). Regions of the PPII,  $\beta$ -strand, and right and left  $\alpha$  helix ( $\alpha_R$ ,  $\alpha_L$ ) are indicated. Values from ref 3 are also shown for comparison (striped-gray rectangles, except for part a, conditions for which no data were available). (a–c) AHA at pD 1.2, 4.4, and 8.0. (d,e) AKA at pD 1.4 and 7.4.

with hydrophobic or hydrophilic side groups and in differently charged states has demonstrated that none of these factors significantly changes the value of the coupling  $\beta$  with respect to the value in diglycine. This is confirmed by calculations in which diglycine-based mappings for the coupling were successfully transferred to larger systems, in particular, a pentapeptide<sup>48</sup> and two globular proteins.<sup>48</sup>

From Figure 10, it can be seen that the mapping ( $\beta, \theta$ )  $\rightarrow$  ( $\phi, \psi$ ) is generally not unique, as there are several ( $\phi, \psi$ ) coordinates at which ( $\beta, \theta$ ) contours intersect. The number of possible ( $\phi, \psi$ ) combinations is reduced because some of the corresponding conformations are not possible because of sterical hindrance. It should be noted that the measurements presented are invariant under the transformation ( $\beta, \theta$ )  $\rightarrow$  ( $-\beta, 180^\circ - \theta$ ), so both pairs of values are taken into account in the analysis.

We used the confidence limits of  $\beta$  and  $\theta$  to determine upper and lower boundary values of the dihedral angles. In this way, we can define confidence regions for the tripeptide conformations in the ( $\phi, \psi$ ) map based on the output of the fit. These regions are shown in Figure 11 for both peptides at the different pD values at which they were studied. The dark-red zone corresponds to the ( $\beta, \theta$ ) values, and the light-red zone is for ( $-\beta, 180^\circ - \theta$ ). The allowed zones calculated from sterical hindrance considerations<sup>49</sup> are shown in blue. These calculations consider only repulsion between atoms modeled as hard spheres for Ala residues. The fully allowed zone is shown in dark blue,

and the partially allowed zone is shown in light blue; they were taken from ref 41. The  $(\varphi, \psi)$  values from ref 3 are also shown as striped-gray rectangles. The first thing from this Figure that catches the eye is the non-Gaussian shape of the  $(\varphi, \psi)$  confidence region obtained from the fits. This is due to the nonlinearity of the  $(\varphi, \psi) \rightarrow (\beta, \theta)$  mapping. It is clear that for a given  $(\beta, \theta)$  there is a strong correlation between  $\varphi$  and  $\psi$ . It can be also noticed that very little to no overlap between the red and blue areas exists in the  $\alpha$ -helical region (light red), so that an  $\alpha$ -helical configuration can be excluded. The situation is different in the upper left area, where the only overlap with the fully allowed zone occurs for  $(\varphi, \psi)$  values corresponding to the PPII (polyproline II) conformation, and overlap with the partially allowed zone occurs for  $(\varphi, \psi)$  values corresponding to the  $\beta$ -strand conformation, for both AHA and AKA.

The confidence regions we find for the dihedral angles of AHA and AKA are close to the values found by Eker et al.<sup>3</sup> for all pD values. Nevertheless, there are some differences between the results obtained with the two approaches, particularly regarding the pD dependence. For AHA at pD 1.2, the confidence regions are in overlap in both the PPII and the  $\beta$ -strand zones. (This pD was not measured in ref 3.) When the pD is increased to 4.4, the confidence regions become smaller, and our results are in agreement with those of Eker et al. This overlap happens in the PPII zone. However, when the pD is increased to 8.0, Eker et al. found a preferred conformation of AHA in the  $\beta$ -strand zone, and although our result is also more suggestive of that conformation (larger confidence region), there is no clear preference for either of the two. For AKA, the situation is similar: Eker et al. found that the preferred conformation changes from the PPII to  $\beta$ -strand when going from pD 1.4 to 7.4, but we find very similar confidence regions for these two pD values. Although both methods for determining the dihedral angles of tripeptides are equally commendable, there are apparently small discrepancies in the predicted conformations. One explanation for the different results might be that contrary to what we assumed in our model a significant fraction of the peptide molecules is in a different conformation. In that case, the observed coupling and dipole–dipole angle are weighted averages over the different conformations, where the weighting function depends on the experimental method employed. It has recently been demonstrated that this ambiguity can be resolved by combining IR and Raman spectroscopy with additional experimental methods.<sup>29–31,50</sup>

Our results show that the conformation of AKA and AHA are insensitive to the pD and hence to the charges on the terminal carboxylate and side-chain groups. It is important to remark that this conclusion does not depend on our assumption used in the quantitative modeling that the peptide is mainly in one conformation. In the case that a distribution of several conformers would exist, our measurements would be an average over this distribution. The observed  $(\beta, \theta)$  would then be averages of the different  $(\beta_i, \theta_i)$  of each conformer  $i$  in the distribution, each weighted with a value determined by its relative population. It should be noted that the weights would not be equal to the relative populations because of the nonlinear relation between  $(\beta, \theta)$  and the measured 2D spectra: the coupling appears as the cross-peak intensity, which depends on it approximately quadratically, and the dipole–dipole angle  $\theta$  appears as the cross-peak anisotropy  $R$ , which is related to it by  $R = (1/5)(3 \cos^2 \theta - 1)$ .<sup>5</sup> It is not likely that a  $(\beta, \theta)$  pair obtained from such an averaging would correspond to a (sterically allowed)  $(\varphi, \psi)$  conformation, as the observed  $(\beta, \theta)$  pair does. Hence, significant population of more than one conformer is not likely, but even

if such a distribution would exist, then our data shows that this distribution does not change with pD. If it would, then the observed average  $(\beta, \theta)$  values would change with pD. On the contrary, we obtained, within the limits of our method, the same  $(\beta, \theta)$  pair for all pD values at which we measured, so we can conclude that the distribution of conformers does not change upon changing the charges on the terminal and side chain groups.

A probable explanation for the insensitivity of the peptide conformation to the side-group and C-terminal charges is that the electrostatic interaction between these charged groups is efficiently screened by the water molecules between them. In some peptides, electrostatic interaction between charged groups (salt bridges) plays a role in determining the backbone conformation. However, the electrostatic interaction has to compete energetically with solvation interactions. As a consequence, electrostatic interactions influence the conformation mainly if the solvation interaction is comparatively small, as is the case when the charged groups are buried in the inside of a protein.<sup>51,52</sup> In small peptides, it may be expected that the free-energy contribution of the solvation is larger than that of the electrostatic interaction. In fact, in a pentapeptide containing a lysine side chain and a C-terminal carboxylate group, formation of a  $\text{Lys}^+ \cdot \text{COO}^-$  salt bridge is observed only in octanol (where the free energy of the salt bridge is larger than that of the solvation of the charged side groups), whereas in water, no salt bridge is formed. This shows that in aqueous solution the free energy of the electrostatic interaction is smaller than that of the solvation of the charged side groups.<sup>53</sup> Our results suggest that this is also the case for the tripeptides investigated here.

In conclusion, we have studied the conformation of the tripeptides AHA and AKA in aqueous solution using 2DIR spectroscopy and an excitonic model for the coupling between Amide I' modes. We find that the dihedral angles  $(\varphi, \psi)$  of these tripeptides do not change significantly upon protonation of their side-chains or C-terminal carboxylate groups. We also find that the highly nonlinear relation between the observables  $(\beta, \theta)$  and the dihedral angles leads to a complicated confidence region for these angles in which there is a significant correlation between  $\varphi$  and  $\psi$ . It should be realized that any spectroscopic method that uses intramolecular couplings (even between spins, like NMR<sup>54</sup>) will be intrinsically limited by the same (or similar) considerations.

**Acknowledgment.** We gratefully acknowledge P. Hamm for providing us with the results of his calculations and Alexander Vdovin for his aid with the calculations on the glycine trimer. We would also like to thank W. J. Buma and R. Schweitzer-Stenner for reading the manuscript. This work was financially supported by The Netherlands Organisation for Scientific Research (NWO). S. Woutersen would like to acknowledge the European Research Council (ERC) for funding through ERC starting grant 210999.

## References and Notes

- Wright, P. E.; Dyson, H. J.; Lerner, R. A. *Biochemistry* **1988**, 27, 7167–7175.
- Eker, F.; Cao, X.; Nafie, L.; Schweitzer-Stenner, R. *J. Am. Chem. Soc.* **2002**, 124, 14330–14341.
- Eker, F.; Griebel, K.; Cao, X.; Nafie, L. A.; Schweitzer-Stenner, R. *Proc. Natl. Acad. Sci. U.S.A.* **2004**, 101, 10054–10059.
- Schweitzer-Stenner, R. *Vib. Spectrosc.* **2006**, 42, 98–117.
- Hamm, P.; Lim, M.; Hochstrasser, R. M. *J. Phys. Chem. B* **1998**, 102, 6123–6138.
- Hamm, P.; Degrado, M. L. W. F.; Hochstrasser, R. M. *Proc. Natl. Acad. Sci. U.S.A.* **1999**, 96, 2036–2041.

- (7) Asplund, M. C.; Zanni, M. T.; Hochstrasser, R. M. *Proc. Natl. Acad. Sci. U.S.A.* **2000**, *97*, 8219–8224.
- (8) Woutersen, S.; Hamm, P. *J. Phys. Chem. B* **2000**, *104*, 11316–11320.
- (9) Demirdöven, N.; Cheatum, C. M.; Chung, H. S.; Khalil, M.; Knoester, J.; Tokmakoff, A. *J. Am. Chem. Soc.* **2004**, *126*, 7981–7990.
- (10) Jansen, T. I. C.; Knoester, J. *J. Phys. Chem. B* **2006**, *110*, 22910–22916.
- (11) Smith, A. W.; Tokmakoff, A. *J. Chem. Phys.* **2007**, *126*, 045109.
- (12) Ganim, Z.; Chung, H. S.; Smith, A. W.; DeFlores, L. P.; Jones, K. C.; Tokmakoff, A. *Acc. Chem. Res.* **2008**, *41*, 432–441.
- (13) DeFlores, L. P.; Ganim, Z.; Nicodemus, R. A.; Tokmakoff, A. *J. Am. Chem. Soc.* **2009**, *131*, 3385–3391.
- (14) Shim, S.-H.; Gupta, R.; Ling, Y. L.; Strasfeld, D. B.; Raleigh, D. P.; Zanni, M. T. *Proc. Natl. Acad. Sci. U.S.A.* **2009**, *106*, 6614–6619.
- (15) Fraser, P. E.; Nguyen, J. T.; Surewicz, W. K.; Kirschner, D. A. *Biophys. J.* **1991**, *60*, 1190–1201.
- (16) Wood, S.; Maleeff, B.; Hart, T.; Wetzel, R. *J. Mol. Biol.* **1996**, *256*, 870–877.
- (17) Picotti, P.; De Franceschi, G.; Frare, E.; Spolaore, B.; Zambonin, M.; Chiti, F.; de Laureto, P.; Fontana, A. *J. Mol. Biol.* **2007**, *367*, 1237–1245.
- (18) Sieler, G.; Schweitzer-Stenner, R.; Holtz, J. S. W.; Pajcini, V.; Asher, S. A. *J. Phys. Chem. B* **1999**, *103*, 372–384.
- (19) Schweitzer-Stenner, R.; Eker, F.; Huang, Q.; Griebenow, K. *J. Am. Chem. Soc.* **2001**, *123*, 9628–9633.
- (20) Schweitzer-Stenner, R. *Biophys. J.* **2002**, *83*, 523–532.
- (21) Schweitzer-Stenner, R. *J. Phys. Chem. B* **2004**, *108*, 16965–16975.
- (22) Krimm, S.; Bandekar, J. *Adv. Protein Chem.* **1986**, *38*, 181–364.
- (23) Richardson, J. S. *Adv. Protein Chem.* **1981**, *34*, 167–339.
- (24) Ford, S. J.; Wen, Z. Q.; Hecht, L.; Barron, L. D. *Biopolymers* **1994**, *34*, 303–313.
- (25) Li, N. C.; Tang, P.; Mathur, R. *J. Phys. Chem.* **1961**, *65*, 1074–1076.
- (26) Woutersen, S.; Hamm, P. *J. Chem. Phys.* **2001**, *114*, 2727–2737.
- (27) Dawson, R.; Elliot, D.; Elliot, W.; Jones, K. *Data for Biochemical Research*, 2nd ed.; Oxford University Press: New York, 1969.
- (28) Barth, A. *Prog. Biophys. Mol. Biol.* **2000**, *74*, 141–173.
- (29) Graf, J.; Nguyen, P. H.; Stock, G.; Schwalbe, H. *J. Am. Chem. Soc.* **2007**, *129*, 1179–1189.
- (30) Hagarman, A.; Measey, T. J.; Mathieu, D.; Schwalbe, H.; Schweitzer-Stenner, R. *J. Am. Chem. Soc.* **2010**, *132*, 540–551.
- (31) Pizzanelli, S.; Forte, C.; Monti, S.; Zandomeneghi, G.; Hagarman, A.; Measey, T. J.; Schweitzer-Stenner, R. *J. Phys. Chem. B* **2010**, *114*, 3965–3978.
- (32) Torii, H.; Tasumi, M. *J. Chem. Phys.* **1991**, *96*, 3379–3387.
- (33) Torii, H.; Tasumi, M. *J. Chem. Phys.* **1992**, *97*, 86–91.
- (34) Huang, Q.; Schweitzer-Stenner, R. *J. Raman Spectrosc.* **2004**, *35*, 586–591.
- (35) Mukamel, S. *Principles of Nonlinear Optical Spectroscopy*; Oxford University Press: New York, 1995.
- (36) Kubo, R.; Hashitsume, N. *Statistical Physics II: Nonequilibrium Statistical Mechanics*; Springer: Berlin, 1985.
- (37) Press, W. H.; Teukolsky, S. A.; Vetterling, W. T.; Flannery, B. P. *Numerical Recipes in C: The Art of Scientific Computing*, 2nd ed.; Cambridge University Press: New York, 1997; Chapter 15.
- (38) Chelli, R.; Volkov, V. V.; Righini, R. *J. Comput. Chem.* **2008**, *29*, 1507–1516.
- (39) Larsen, O. F. A.; Bodis, P.; Buma, W. J.; Leigh, D. A.; Woutersen, S. *Proc. Natl. Acad. Sci. U.S.A.* **2005**, *102*, 13378–13382.
- (40) Hamm, P.; Woutersen, S. *Bull. Chem. Soc. Jpn.* **2002**, *75*, 985–988.
- (41) Creighton, T. E. *Proteins: Structures and Molecular Properties*; W. H. Freeman and Company: New York, 1984.
- (42) Torii, H.; Tasumi, M. *J. Raman Spectrosc.* **1998**, *29*, 81–86.
- (43) Hamm, P.; Woutersen, S. *Bull. Chem. Soc. Jpn.* **2002**, *75*, 985–988.
- (44) Cha, S.; Ham, S.; Cho, M. *J. Chem. Phys.* **2002**, *117*, 740–750.
- (45) Antony, J.; Schmidt, B.; Schütte, C. *J. Chem. Phys.* **2005**, *122*, 014309.
- (46) Gorbunov, R. D.; Kosov, D. S.; Stock, G. *J. Chem. Phys.* **2005**, *122*, 224904.
- (47) Jansen, T. L.; Dijkstra, A. G.; Watson, T. M.; Hirst, J. D.; Knoester, J. *J. Chem. Phys.* **2006**, *125*, 044312.
- (48) Choi, J.-H.; Ham, S. Y.; Cho, M. *J. Chem. Phys.* **2002**, *117*, 6821–6832.
- (49) Ramachandran, G. N.; Sasisekharan, V. *Adv. Protein Chem.* **1968**, *23*, 283–438.
- (50) Schweitzer-Stenner, R.; Measey, T.; Kakalis, L.; Jordan, F.; Pizzanelli, S.; Forte, C.; Griebenow, K. *Biochemistry* **2007**, *46*, 1587–1596.
- (51) Anderson, D.; Becktel, W.; Dahlquist, F. *Biochemistry* **1990**, *29*, 2403–2408.
- (52) Waldburger, C. D.; Schildbach, J. F.; Sauer, R. T. *Nat. Struct. Biol.* **1995**, *2*, 122–128.
- (53) Wimley, W. C.; Gawrisch, K.; Creamer, T. P.; White, S. H. *Proc. Natl. Acad. Sci. U.S.A.* **1995**, *93*, 2985–2990.
- (54) Weliky, D. P.; Tycko, R. *J. Am. Chem. Soc.* **1996**, *118*, 8487–8488.

JP105133R